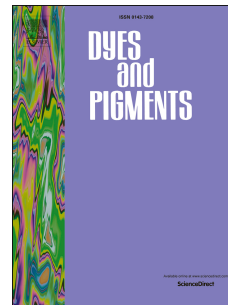


Accepted Manuscript

A new series of azobenzene-bridged metal-free organic dyes and application on DSSC

Kuo Yuan Chiu, Thai Thi Ha Tran, Sheng Hsiung Chang, Te-Fang Yang, Yuhlong Oliver Su



PII: S0143-7208(17)30633-2

DOI: [10.1016/j.dyepig.2017.07.049](https://doi.org/10.1016/j.dyepig.2017.07.049)

Reference: DYPI 6138

To appear in: *Dyes and Pigments*

Received Date: 17 April 2017

Revised Date: 21 July 2017

Accepted Date: 21 July 2017

Please cite this article as: Chiu KY, Ha Tran TT, Chang SH, Yang T-F, Su YO, A new series of azobenzene-bridged metal-free organic dyes and application on DSSC, *Dyes and Pigments* (2017), doi: 10.1016/j.dyepig.2017.07.049.

This is a PDF file of an unedited manuscript that has been accepted for publication. As a service to our customers we are providing this early version of the manuscript. The manuscript will undergo copyediting, typesetting, and review of the resulting proof before it is published in its final form. Please note that during the production process errors may be discovered which could affect the content, and all legal disclaimers that apply to the journal pertain.

A New Series of Azobenzene-bridged Metal-free Organic Dyes and Application on DSSC

Kuo Yuan Chiu,^a Thai Thi Ha Tran,^a Sheng Hsiung Chang,^b Te-Fang Yang,^{a,**}
Yuhlong Oliver Su^{a,*}

^a Department of Applied Chemistry, National Chi Nan University, 1 University Road, Puli, Nantou 545, Taiwan

^b Research Center for New Generation Photovoltaics, National Central University, No.300, Zhongda Rd., Zhongli City, Taoyuan 320, Taiwan

Corresponding Author

** Email: tfyang@ncnu.edu.tw

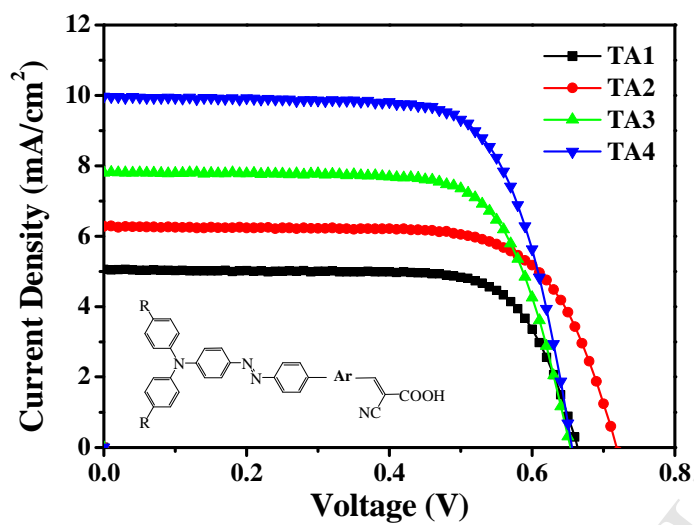
* Email: yosu@nchu.edu.tw

Keywords: DSSC • Organic dye • Azobenzene • Electrochemistry • DFT

Abstract

A series of novel azobenzene-based dyes were designed and synthesized using azobenzene as the π -spacer unit to connect diarylamino and cyanoacetic acids for construction of the D- π -A conformation. The introduction of a thienyl into the anchor group (A) could lead to a red-shift in the absorption spectra and λ_{onset} of the dyes. When the diarylamino substituent was changed from methyl to methoxyl, a slight negative shift in the first oxidation peak could be observed. The spin density distribution of the cation radicals of the four dyes was also investigated. The qualitative order of the stability of these four cation radicals was found to be **TA4** > **TA3** > **TA2** > **TA1** in air. They were then employed as the sensitizer in organic dye-sensitized solar cells to achieve the highest power conversion efficiency (PCE) of 4.78 % under AM 1.5 conditions. By systematically changing the donor and acceptor unit of these dyes, the new record on PCE with using azobenzene as the π -spacer unit was achieved.

Graphical abstract



Highlights

- A series of novel azobenzene-based dyes were synthesized.
- The stability order of these four dyes cation radicals was found to be **TA4 > TA3 > TA2 > TA1** in air.
- The new record on PCE with using azobenzene as the π -spacer unit was achieved.

1. Introduction

Recently, numerous metal-free organic dyes have been introduced for use in solar cells which have the advantages of a wide variety of structural designs and high molar absorption coefficients. The resultant solar cells often display respectable power conversion efficiencies (PCE) [1-3]. The Donor-(π -spacer)-Acceptor (D- π -A) system is the basic architecture used for the design of organic sensitizers due to the effective photoinduced intramolecular charge transfer properties [4]. In general, TAA (triarylamine) units are widely used as electron donors due to their strong electron-donating ability. On the other hand, the cyanoacrylic acid moiety is usually employed as the electron acceptor as well as the anchoring group that attaches to the surface of the TiO₂ [1,5].

The use of a suitable electron-rich group as the π -spacer between the electron donor and electron acceptor was reported to be beneficial by inducing a red-shift in absorption maximum during the charge-transfer transition [6-8]. Many studies have focused on the conjugate chains such as vinyl [6], stilbene [7], anthracene [8], phenyl and thienyl. However, the use of azobenzene as the π -spacer in the D- π -A structure for metal-free organic dyes has not been studied in detail thus far. The azobenzene derivatives have revealed a number of important characteristics, such as thermal stability over a wide temperature range [9], high chemical stability, stronger electronic communication [10] and lower optical band gap (LUMO-HOMO), when the azobenzene moiety is used for bridge conformation [11]. To the best of our knowledge, there have been few reports of the construction of sensitizers comprised of azobenzene units, even though they have shown very low PCE [12,13]. We herein report a facile synthesis and the application of four novel organic dyes (**TA1-TA4**, Scheme 1), in which diarylamine is used as the electron-donating moiety, azobenzene moiety as the π -spacer, and aromatic-cyanoacrylic acid as the anchoring moiety

(Figure 1). The best PCE is almost four times greater than the previous studies [12].

2. Experimental

2.1. Materials and physicochemical study

All chemicals used were obtained from the commercial resources and used as received unless specified. HPLC grade CH_2Cl_2 was purchased from ACROS and was distilled from CaH_2 under an argon (Ar) atmosphere for electrochemical use. Tetra-*n*-butylammonium hexafluorophosphate (TBAPF_6) was recrystallized twice from ethanol and then stored in a desiccator. $^1\text{H-NMR}$ and $^{13}\text{C-NMR}$ spectra were recorded with a Bruker 300 MHz NMR spectrometer using CDCl_3 as a solvent. FAB-MS spectra were obtained using JMS-700 spectrometer. UV/Vis absorption and emission spectra were measured using a Cary 300 Bio spectrophotometer and FluoroMax-4 spectrofluorometer (HORIBA JOBIN YVON), respectively. Elemental analyses were carried out with a Heraeus CHN-O-S Rapid-F002 analysis system. Electrochemistry was conducted using a three-electrode cell with BAS glassy carbon working electrode (GCE, area = 0.07 cm^2). The glassy carbon electrode was polished with $0.05 \mu\text{m}$ alumina on Buehler felt pads and was ultrasonicated for 2 min to remove the alumina residue. A platinum wire was used as the auxiliary electrode. A home-made Ag/AgCl, KCl (saturated) was the reference electrode. The supporting electrolyte was 0.1 M tetrabutylammonium hexafluorophosphate (TBAPF_6) in CH_2Cl_2 . The square-wave voltammograms (frequency: 25 Hz; step potential: 0.0051 V; amplitude: 0.01995 V) were recorded using a potentiostat/ galvanostat (PGSTAT 30, Autolab, Eco-Chemie, the Netherlands) and ferrocene was used as a calibration standard (+0.49 V versus Ag/AgCl).

2.2. Synthesis of TA1, TA2, TA3 and TA4

Compounds **1**, **2**, **3**, **4**, and 1-bromo-4-nitrosobenzene were synthesized according to the previous reports [14,15]. The synthesis pathway of **TA** series are shown in Scheme 1.

Synthesis of compound 5. 1-Bromo-4-nitrosobenzene (3.45 g, 18.5 mmol, 1eq.) was dissolved in a mixture of acetic acid / ethyl acetate 1/1 (200 mL). To this solution, **3** (4.28 g, 14.83 mmol, 0.8 eq.) was added directly. The reaction mixture was stirred at 40 °C overnight. After cooling to room temperature, a precipitate appeared. The precipitate was filtered and purified by silica-gel column chromatography using CH₂Cl₂/hexane (1:1) as the eluent to afford compound **5** as a dark yellow solid (yield: 80.2%), m.p. 176-178 °C. IR (KBr), cm⁻¹: 2916、1590、1505、1484、1316、1294、1267、1135、1065、1002、836、809. ¹H NMR (300 MHz, CDCl₃) δ 7.77-7.71 (m, 4H), 7.65-7.58 (m, 2H), 7.14-7.00 (m, 10H), 2.34 (s, 6H). ¹³C NMR (75 MHz, CDCl₃) δ 152.0, 151.5, 146.5, 144.4, 134.4, 132.4, 132.3, 130.4, 127.5, 126.1, 124.6, 124.2, 120.2, 21.1. MS (FAB⁺) *m/z* Calcd for C₂₆H₂₂BrN₃, ([M + H]⁺) 455.0997, 457.0977; found, 455.0999, 457.0981.

Synthesis of compound 6. 1-Bromo-4-nitrosobenzene (3.45 g, 18.5 mmol, 1eq.) was dissolved in a mixture of acetic acid / ethyl acetate 1/1 (200 mL). To this solution, **4** (4.75 g, 14.83 mmol, 0.8 eq.) was added directly. The reaction mixture was stirred at 40 °C overnight. After cooling to room temperature, a precipitate appeared. The precipitate was filtered and purified by silica-gel column chromatography using CH₂Cl₂/hexane (1:1) as the eluent to afford compound **6** as a orange-red solid (yield: 85.1%), m.p. 169-171 °C. IR (KBr), cm⁻¹: 2997、1593、1508、1316、1288、1234、1132、1023、824. ¹H NMR (300 MHz, CDCl₃) δ 7.73 (t, *J* = 7.5 Hz, 6.9 Hz, 4H), 7.58 (d, *J* = 6.9 Hz, 2H), 7.13 (d, *J* = 6.6 Hz, 4H), 6.94-6.85 (m, 6H), 3.81 (s, 6H). ¹³C NMR (75 MHz, CDCl₃) δ 157.0, 152.0, 151.6, 146.0, 139.8, 132.4, 127.8, 124.7,

124.1, 118.6, 115.1, 55.7. MS (FAB⁺) m/z Calcd for C₂₆H₂₂BrN₃O₂, ([M + H]⁺) 487.0895, 489.0875; found, 487.0901, 489.0877.

Synthesis of compound 5a. Compound **5** (27.3 mg, 6×10⁻² mmol) and 4-formylphenylboronic acid (13 mg, 9×10⁻² mmol) were dissolved in anhydrous toluene (10 mL), then Pd(PPh₃)₄ (17 mg, 1.5×10⁻² mmol) and Na₂CO₃ (63.6 mg, 6×10⁻¹ mmol) in water (5 mL) was added as a catalyst. The mixture was refluxed under argon for 24 hours. After cooling to the room temperature, the crude compound was extracted by ethyl acetate/water, then washed with brine and finally dried with an anhydrous sodium sulfate. The solution was concentrated under reduced pressure and the residue was purified by column chromatography (CH₂Cl₂/hexane = 2:1, v/v) on a silica gel to yield a red powder **5a** (80% yield), m.p. 182-183 °C. IR (KBr), cm⁻¹: 3018, 1686, 1593, 1499, 1406, 1312, 1288, 1207, 1138, 824. ¹H NMR (300 MHz, CDCl₃) δ 10.07 (s, 1H), 7.99-7.95 (m, 4H), 7.84-7.75 (m, 6H), 7.15-7.04 (m, 10H), 2.35 (s, 6H). ¹³C NMR (75 MHz, CDCl₃) δ 192.1, 146.8, 146.6, 144.4, 134.4, 130.6, 130.4, 128.3, 127.9, 126.1, 124.6, 123.3, 120.3, 21.15. MS (FAB⁺) m/z Calcd for C₃₃H₂₇N₃O, ([M + H]⁺) 481.2154; found, 481.2155.

Synthesis of compound 6a. The synthesis method resembles that of compound **5a** and the compound was purified by silica-gel column chromatography using CH₂Cl₂/hexane (1:1) as the eluent to afford compound **6a** as a yellow solid (yield: 40.2%), m.p. 177-178 °C. IR (KBr), cm⁻¹: 3020, 1698, 1587, 1499, 1328, 1240, 1135, 1020, 824. ¹H NMR (300 MHz, CDCl₃) δ 10.05 (s, 1H), 7.97-7.93 (m, 4H), 7.81-7.73 (m, 6H), 7.14-7.11 (d, $J = 8.4$ Hz, 4H), 6.95 (d, $J = 9$ Hz, 2H), 6.86 (d, $J = 8.7$ Hz, 4H), 3.81 (s, 6H). ¹³C NMR (75 MHz, CDCl₃) δ 192.1, 157.0, 153.1, 151.9, 146.6, 146.2, 140.9, 139.8, 135.6, 130.5, 128.2, 127.8, 124.7, 123.3, 118.6, 115.1, 55.9. MS (FAB⁺) m/z Calcd for C₃₃H₂₇N₃O₃ ([M + H]⁺) 513.2052; found, 513.2050.

Synthesis of compound 5b. Compound **5** (27.3 mg, 6×10^{-2} mmol) and 5-Formyl-2-thienylboronic acid (14 mg, 9×10^{-2} mmol) were dissolved in anhydrous toluene (10 mL), then Pd(PPh₃)₄ (17 mg, 1.5×10^{-2} mmol) and Na₂CO₃ (63.6 mg, 6×10^{-1} mmol) in water (5 mL) was added as a catalyst. The mixture was refluxed under argon for 24 hours. After cooling to the room temperature, the crude compound was extracted by ethyl acetate/water, then washed with brine and finally dried with an anhydrous sodium sulfate. The solution was concentrated under reduced pressure and the residue was purified by column chromatography (CH₂Cl₂/hexane = 2:1, v/v) on a silica gel to yield a dark red powder **5b** (yield: 88%), m.p. 186-187 °C. IR (KBr), cm⁻¹: 2910, 1665, 1590, 1508, 1319, 1270, 1229, 1147, 1056, 839, 809. ¹H NMR (300 MHz, CDCl₃) δ 9.90 (s, 1H), 7.91-7.77 (m, 6H), 7.46-7.40 (m, 2H), 7.11-7.02 (m, 10H), 2.34 (s, 6H). ¹³C NMR (75 MHz, CDCl₃) δ 183.0, 153.6, 153.5, 151.6, 146.7, 144.3, 143.0, 137.6, 134.5, 134.4, 130.4, 129.4, 127.2, 126.6, 126.1, 124.7, 124.3, 123.5, 120.2, 21.1. MS (FAB⁺) *m/z* Calcd for C₃₁H₂₅N₃OS, ([M + H]⁺) 487.1718; found, 487.1720.

Synthesis of compound 6b. The synthesis method resembles that of compound **5b** and the compound was purified by silica-gel column chromatography using CH₂Cl₂/hexane (1:1) as the eluent to afford compound **6b** as a yellow solid (yield: 40.2%), m.p. 153-155 °C. IR (KBr), cm⁻¹: 2922, 1737, 1656, 1508, 1243, 1035, 855, 822. ¹H NMR (300 MHz, CDCl₃) δ 9.89 (s, 1H), 7.89 (d, *J* = 8.1 Hz, 2H), 7.78-7.76 (m, 6H), 7.13 (d, *J* = 8.7 Hz, 4H), 6.93 (d, *J* = 9 Hz, 2H), 6.87 (d, *J* = 9 Hz, 4H), 3.81 (s, 6H). ¹³C NMR (75 MHz, CDCl₃) δ 183.0, 157.1, 153.7, 153.6, 152.0, 146.2, 143.0, 139.8, 137.6, 137.1, 134.2, 127.8, 127.2, 124.8, 124.7, 123.4, 118.5, 115.1, 55.7. MS (FAB⁺) *m/z* Calcd for C₃₁H₂₅N₃O₃S, 519.1617; found, 519.1621.

Synthesis of TA1. An oven-dried 100 mL one-necked flask was charged with compound **5** (3.5×10^{-1} mmol), cyanoacrylic acid (7 mmol), dry THF (10 mL) and piperidine (0.4 mL). The solution was heated at reflux for 15 h and the color turned deep red. After cooling to room temperature, dichloromethane was added and the organic phase was washed with water (3×20 mL) and brine (3×20 mL). The combined organic phase was dried on MgSO₄, filtered and evaporated under reduced pressure and the residue was purified by silica-gel column chromatography to give a purple solid (86.5%), m.p. 197-198 °C. IR (KBr), cm⁻¹: 3033, 1590, 1505, 1319, 1138, 818. ¹H NMR (300 MHz, CDCl₃) δ 8.14 (br, 1H), 7.72-7.55 (m, 2H), 7.58-7.56 (d, $J = 8.1$ Hz, 6H), 6.96 (d, $J = 8.4$ Hz, 4H), 6.86 (d, $J = 8.1$ Hz, 6H), 2.24 (s, 6H). ¹³C NMR (75 MHz, CDCl₃) δ 210.2, 171.0, 144.6, 137.3, 134.6, 133.8, 130.3, 127.7, 125.8, 124.6, 123.2, 120.6, 21.1. MS (FAB⁺) m/z . Calcd for C₃₆H₂₈N₄O₂, ([M + H]⁺) 548.2212; found, 548.2219.

Synthesis of TA2. The synthesis method resembles that of **TA1** and the compound was purified by silica-gel column chromatography using CH₂Cl₂/MeOH (10:1) as the eluent to afford com **TA2** as a yellow solid (yield: 90%), m.p. 165-167 °C. IR (KBr), cm⁻¹: 3031, 1593, 1508, 1243, 1141, 825. ¹H NMR (300 MHz, CDCl₃) δ 8.17 (br, 1H), 7.94-7.60 (m, 6H), 7.28-7.26 (m, 4H), 6.97 (d, $J = 8.7$ Hz, 4H), 6.77-6.74 (m, $J = 8.7$ Hz, 6H), 3.74 (s, 6H). ¹³C NMR (75 MHz, CDCl₃) δ 195.8, 156.7, 152.6, 151.3, 146.4, 140.4, 140.1, 131.6, 127.7, 127.5, 124.7, 123.2, 119.0, 115.0, 55.6. MS (FAB⁺) m/z . Calcd for C₃₆H₂₈N₄O₄, ([M + H]⁺) 580.2111; found, 580.2115.

Synthesis of TA3. The synthesis method resembles that of **TA1** and the compound was purified by silica-gel column chromatography using CH₂Cl₂/MeOH (10:1) as the eluent to afford **TA3** as a yellow solid (yield: 88.6%), m.p. 173-174 °C. IR (KBr), cm⁻¹: 3019, 2361, 1593, 1511, 1322, 1270, 1129, 842, 824. ¹H NMR (300 MHz, CDCl₃)

δ 8.23 (br, 1H), 7.53 (m, 6H), 7.30 (m, 4H), 7.00-6.85 (m, 8H), 2.26 (s, 6H). ^{13}C NMR (150 MHz, CD_2Cl_2) δ 206.9, 153.1, 151.4, 146.7, 144.5, 136.4, 134.6, 134.29, 130.4, 127.0, 126.2, 124.7, 123.4, 120.0, 116.3, 110.4, 21.0. MS (FAB⁺) m/z Calcd for $\text{C}_{34}\text{H}_{26}\text{N}_4\text{O}_2\text{S}$, ($[\text{M} + \text{H}]^+$) 554.1776; found, 554.1775.

Synthesis of TA4. The synthesis method resembles that of **TA1** and the compound was purified by silica-gel column chromatography using $\text{CH}_2\text{Cl}_2/\text{MeOH}$ (10:1) as the eluent to afford **TA4** as a yellow solid (yield: 85.9%), m.p. 181-183 °C. IR (KBr), cm^{-1} : 3016, 2361, 1593, 1508, 1237, 1129, 1032, 775. ^1H NMR (300 MHz, CDCl_3) δ 8.28 (br, 1H), 7.45 (m, 4H), 7.15 (m, 2H), 6.91-6.72(m, 12H), 3.70 (s, 6H). ^{13}C NMR (150 MHz, CD_2Cl_2) δ 192.1, 160.9, 157.2, 146.3, 140.0, 138.9, 128.0, 124.8, 123.4, 118.5, 115.2, 55.8. MS (FAB⁺) m/z Calcd for $\text{C}_{34}\text{H}_{26}\text{N}_4\text{O}_4\text{S}$, ($[\text{M} + \text{H}]^+$) 586.1675; found, 586.1669.

2.3. Device fabrication and photovoltaic performance test

Anatase TiO_2 nanoparticles (NP) (ca. 20 nm diameter) were hydrothermally prepared in a Ti based autoclave as reported previously [16]. The screen-printable 20 nm TiO_2 paste was prepared by thoroughly mixing of 4.23 g TiO_2 NP, 55 mL ethyl cellulose, and 45 mL terpineol. The TiO_2 paste was screen-printed to form an active area of 0.16 cm^2 TiO_2 photoanode (11 μm thick mesoporous anatase- TiO_2 film and 4 μm thick TiO_2 scattering layer with particle size of ca. 400 nm) on the fluorine-doped tin oxide glass (FTO glass, $7 \Omega/\text{square}$, 2.2 mm thick) with pretreatment with 40 mM $\text{TiCl}_{4(\text{aq})}$ at 70 °C for 30 min and control the thickness. Then the TiO_2 electrodes were heated under an air flow at 500 °C for 60 minutes. After cooling to room temperature, the TiO_2 electrode was immersed in the TEDBn or TEDTh organic sensitizer solution (0.2 mM) with 20 mM chenodeoxycholic acid (CDCA, Sigma-Aldrich) in THF at 40°C for 3 hours, and then rinsed with acetonitrile. The cell was covered with

platinized FTO glass incorporating a drilled hole, to form the counter electrode and complete the sandwich configuration. The cell interior was separated by a 30 μm surlyn and the electrolyte was injected into the cell *via* the hole in the counter electrode. The electrolyte was composed of BMII (0.6 M), LiI (0.1 M), *tert*-butylpyridine (TBP, Sigma-Aldrich) (0.5 M), 0.1 M GuNCS and I₂ (0.05 M) in acetonitrile. Finally, drill holes were sealed using Surlyn hot-melt polymer and cover glass.

Light illumination for the photovoltaic measurements employed a 100 mW/cm² simulated Sun light source (Yamashita Denso, YSS-50A), and the light-source power output was calibrated using a reference Si photodiode (BS-520, Bunko Keiki). The DSC photovoltaic characteristics were obtained by applying an external potential bias to the cell, and measuring the generated photocurrent using a Keithley model 2400 digital source meter (Keithley, USA). Photocurrent action spectra for the incident monochromatic photon to current conversion efficiency (IPCE) were taken with an IPCE measurement system (EQE-R-3011, ENLI Technology Co. Ltd., Taiwan) calibrated with a single-crystal silicon reference cell for each measurement.

3. Results and discussion

The absorption spectra of **TA1-TA4** in CH₃CN are shown in Figure 2. It can be seen that the main absorption wavelength in CH₃CN is between 400 and 650 nm, as contributed by the azobenzene π -spacer. This allows the efficient absorption of photons with lower energy [17]. The onset value of the visible absorption maxima (λ_{onset}) of the dyes corresponds to the energy gap (E_{0-0}) between the HOMO to LUMO transitions (Table 2) [18]. With the change in the diarylamino group from methyl (**TA1**) to methoxyl (**TA2**), there is a red shift in the value of λ_{onset} . This phenomena can also be observed in **TA3** and **TA4**. A comparison of **TA1** with **TA3** shows that the

introduction of a 2,5-thienyl moiety into the anchor group can lead to a red-shift in the absorption spectra and λ_{onset} (from 610 nm to 660 nm) of the dye, which is desirable for a lower energy gap and for harvesting more solar energy [17].

The first oxidation potential (E_{ox}) of these dyes was measured by square wave voltammetry (SWV) in CH_3CN (Table 1), and was shown to correspond to the HOMO level (Table 2). The E_{ox} of the dyes **TA1**, **TA2**, **TA3** and **TA4** were +1.05, +1.04, +1.08 and +1.06 V vs NHE, respectively. When the diarylamino substituent was changed from methyl to methoxyl (compare **TA1** with **TA2**), only a slight negative shift in the first oxidation peak was observed. The values of E_{ox} for all the dyes were more positive than the potential of the $I/I^{\cdot-}$ redox mediator (~ 0.4 V vs NHE) when employed as an electrolyte in DSCs [19-21].

The LUMO levels of these dyes were calculated by $E_{\text{ox}}+E_{0-0}$, where E_{0-0} is the optical transition energy of the dyes estimated by the onset value of the absorption spectrum (Table 2). The E_{0-0} values of **TA1**, **TA2**, **TA3** and **TA4** were 2.03, 1.91, 1.88 and 1.82 eV, yielding LUMO levels for these dyes of -3.52, -3.63, -3.70 and -3.74 eV, respectively. The frontier orbital energy levels of the dyes (Figure 3) not only confirmed the facile electron injection from photo-excited sensitizers to the TiO_2 conduction band (E_{cb} , ca. -0.3 V vs NHE, - 4.2 eV vs vacuum) [21], but also revealed that azobenzene, used as the π -spacer, caused lower energy level than the conduction band edge of TiO_2 . For all of the dyes, the process of electron injection into E_{cb} of TiO_2 could be completed for oxidization of the dyes.

Density functional theory (DFT) using the hybrid B3LYP function along with the 6-31G(d,p) basis set was employed to investigate the electronic structures of the four dyes, **TA1**, **TA2**, **TA3**, and **TA4**. At the HOMO level, electrons are delocalized from the donor unit to the π -bridge while at the LUMO level, the electron delocalization is

shown to range from the π -bridge to the acceptor moiety (Figure 3). The trend in the calculated HOMO-LUMO gap matches the experimental data obtained from the CV results. The HOMO-LUMO gap decreased with the addition of one more electron-donating group at the donor unit and/or electron-withdrawing group at the acceptor unit. For example, in the experiments, the HOMO-LUMO gaps of **TA1** and **TA2**, (replacing methyl by methoxyl at the donor moiety), were 2.03 and 1.91 eV, respectively. Those gaps obtained with DFT calculations were 2.41 and 2.32 eV. Similarly, after replacing the 1,4-phenylene by a 2,5-thienyl unit at the acceptor moiety, the HOMO-LUMO gaps of **TA1** and **TA3** were 2.03 and 1.88 eV, respectively, while, they were 2.41 and 2.32 eV based on the DFT calculations. The trend of shown by the calculated ionization potentials was also consistent with that of the oxidation potential obtained from the CV results (Table 2 and Table 3).

The spin density distribution of the cation radicals of the four dyes was also investigated. As shown in Figure 4, delocalization mainly occurred at the donor moiety and the calculated spin density values were at the N_D and C_A positions. The trend of the total spin density values at these two positions followed that of the HOMO-LUMO gap, namely that it decreases with the addition of one more electron-donating group at the donor unit or/and electron-withdrawing group at the acceptor unit. The spin density values can be calculated to show the qualitative order of the stability of these four cation radicals was found to be **TA4** > **TA3** > **TA2** > **TA1** in air [22].

The J - V curves and IPCE spectra of these DSSCs are shown in Figure 5. The detailed photovoltaic parameters are summarized in Table 4. By systematically changing the donor and acceptor unit of these dyes, we can increase the PCE. **TA2** had a higher V_{oc} than the other dyes because it possessed a strong electron-donating

group (-OMe) in the donor unit with phenyl as the anchoring moiety. The IPCE spectra of the DSCs sensitized using dyes with the phenyl anchoring group were comparatively shorter and narrower than those of the DSCs sensitized using dyes with other anchoring groups. The *J-V* curves show a trend that is consistent with the stability of the cation radicals of the dyes as predicted by the DFT calculation. The IPCE for the **TA4**-sensitized cell reached its maximum of 53% at 470 nm, significantly higher than that of the **TA1** based device (36% at 545 nm). In the wavelength range from 300 to 600 nm, the **TA4**-sensitized cell also showed a stronger IPCE than others, resulting in the highest PCE of 4.78%.

4. Conclusion

In conclusion, a new series of unsymmetrical dyes containing electron-abundant azobenzene units (π -spacers) between the diarylamine and the terminal cyanoacetic acid have been studied. With this design we could get a lower LUMO, bathochromic shifts of absorption spectra (small energy gap) and increase the value of the J_{sc} and FF because of the change in the electron-donating group on the diarylamine and the difference in the aromatic group on the anchoring moiety. The improvement of J_{sc} can be attributed to the much broader and red-shift absorption spectra of the dyes with the thiophene moiety on the anchoring group. The highest V_{oc} value was observed when using bis(4-methoxyphenyl)amine as the donor unit and phenyl as the anchoring group. The high PCEs of these dyes constructed with the azobenzene spacer were investigated. The results present a new option for developing colorful azobenzene sensitizers for DSC applications.

Acknowledgement

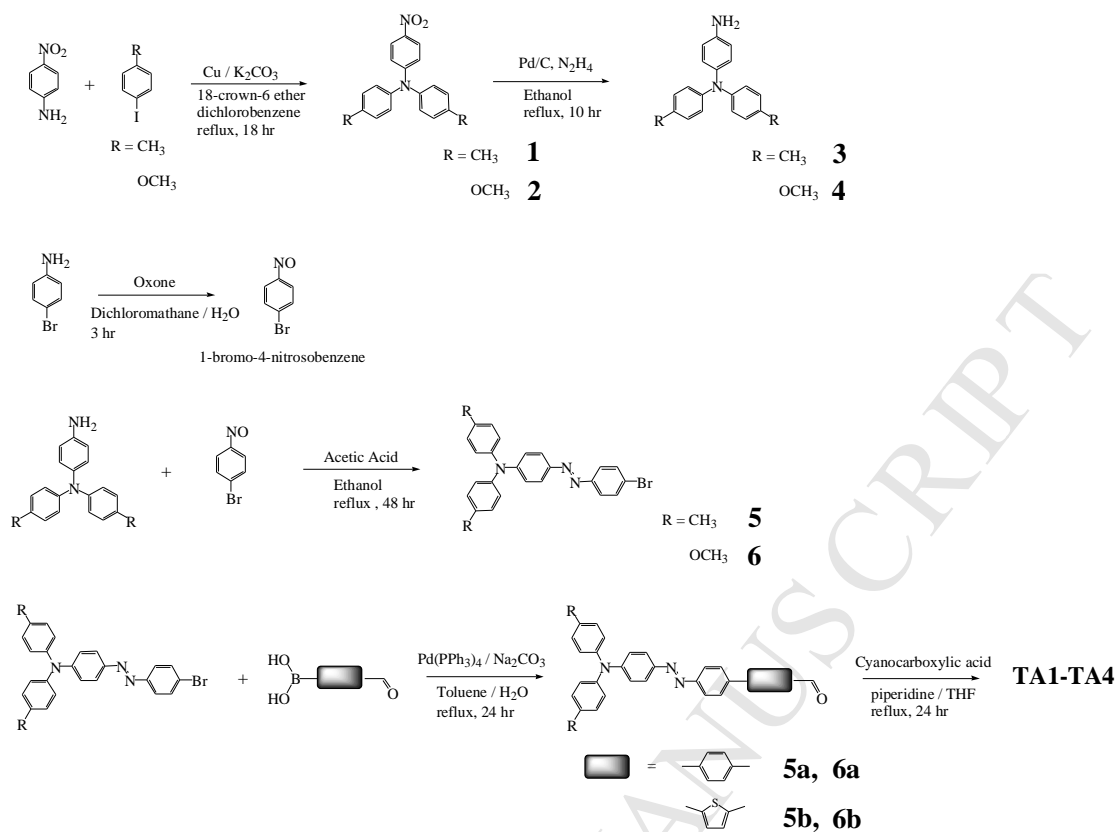
The authors would like to extend their thanks to the Ministry of Science and Technology of Taiwan, R.O.C. for financial support of this work (103-2113-M-260-003 -MY3).

Reference:

- [1] Mishra A, Fischer MKR, Bäuerle P. Metal-free organic dyes for dye-sensitized solar cells: from structure: property relationships to design rules. *Angew Chem Int Ed* 2009; 48(14):2474-99.
- [2] Yan-Duo L, Tahsin JC. Geometrical Effect of Stilbene on the Performance of Organic Dye-Sensitized Solar Cells. *J Mater Chem* 2011; 21: 14907-16.
- [3] Chang YJ, Chow TJ. Dye-sensitized solar cell utilizing organic dyads containing triarylene conjugates. *Tetrahedron* 2009; 65(24): 4726-34.
- [4] Preat J, Michaux C, Jacquemin D, Perpète E. A. Enhanced Efficiency of Organic Dye-Sensitized Solar Cells: Triphenylamine Derivatives. *J Phys Chem C* 2009; 113(38): 16821-33.
- [5] O'Regan B, Grätzel M. A low-cost, high-efficiency solar cell based on dye-sensitized colloidal TiO₂ films. *Nature* 1991; 353: 737-40.
- [6] Teng C, Yang X, Yang C, Tian H, Li S, Wang X, Hagfeldt A, Sun L. Influence of Triple Bonds as π -Spacer Units in Metal-Free Organic Dyes for Dye-Sensitized Solar Cells. *J Phys Chem C* 2010; 114(25): 11305-13.
- [7] Tian H, Yang X, Chen R, Zhang R, Hagfeldt A, Sun L. Effect of Different Dye Baths and Dye-Structures on the Performance of Dye-Sensitized Solar Cells Based on Triphenylamine Dyes. *J. Phys. Chem. C* 2008; 112(29): 11023-33.

- [8] Teng C, Yang X, Yang C, Li S, Cheng M, Hagfeldt A, Sun L. Molecular Design of Anthracene-Bridged Metal-Free Organic Dyes for Efficient Dye-Sensitized Solar Cells. *J Phys Chem C* 2010; 114(19): 9101-10.
- [9] Merino E. Synthesis of azobenzenes: the coloured pieces of molecular materials. *Chem Soc Rev* 2011; 40: 3835-53.
- [10] Screen TEO, Blake IM, Rees LH, Clegg W, Borwick SJ, Anderson HL. Making conjugated connections to porphyrins: a comparison of alkyne, alkene, imine and azo links. *J Chem Soc Perkin Trans* 2002; 1: 320-9.
- [11] Yamamura T, Momotake A, Arai T. Synthesis and photochemical properties of porphyrin-azobenzene triad. *Tetrahedron Lett* 2004; 45(50): 9219-23.
- [12] Unno M, Kakiage K, Yamamura M, Kogure T, Kyomena T, Hanaya M. Silanol dyes for solar cells: higher efficiency and significant durability. *Appl Organometal Chem* 2010; 24(3): 247-50.
- [13] Consiglio GB, Pedna F, Fornaciari C, Biani FFD, Marotta G, Salvatori P, Basosi R, Angelis FD, Mordini A, Parisi ML, Peruzzini M, Reginato G, Taddei M, Zani L. Assessment of new *gem*-silanediols as suitable sensitizers for dye-sensitized solar cells. *J Organometallic Chem* 2013; 723: 198-206.
- [14] Nguyen TTT, Türp D, Wang D, Nölscher B, Laquai F, Müllen K. A Fluorescent, Shape-Persistent Dendritic Host with Photoswitchable Guest Encapsulation and Intramolecular Energy Transfer. *J Am Chem Soc* 2011; 133(29): 11194-204.
- [15] Chiu KY, Su TX, Li JH, Lin TH, Liou GS, Cheng S.-H. Novel trends of electrochemical oxidation of amino-substituted triphenylamine derivatives. *J Electroanal Chem* 2005; 575(1): 95-101.
- [16] Ito S, Murakami TN, Comte P, Liska P, Gratzel C, Nazeeruddin MK, Gratzel M. Fabrication of thin film dye sensitized solar cells with solar to electric power conversion efficiency over 10%. *Thin Solid Film* 2008; 516: 4613-19.

- [17] Zhou L, Jia C, Wan Z, Li Z, Bai J, Zhang L, Zhang J, Yao X. Triphenylamine-based organic dyes containing benzimidazole derivatives for dye-sensitized solar cells. *Dyes and Pigments* 2012; 95: 743-750.
- [18] Lin J, Elangovan A, Ho T. Structure–Property Relationships in Conjugated Donor–Acceptor Molecules Based on Cyanoanthracene: Computational and Experimental Studies. *J Org Chem* 2005; 70(18): 7397-407.
- [19] Li SL, Jiang KJ, Shao KF, Yang LM. Novel organic dyes for efficient dye-sensitized solar cells. *Chem Commun* 2006; 26: 2792-4.
- [20] Kim S, Choi H, Kim D, Song K, Kang SO, Ko J. Novel conjugated organic dyes containing bis-dimethylfluorenyl amino phenyl thiophene for efficient solar cell. *Tetrahedron* 2007; 63(37): 9206-12.
- [21] Chen CY, Pootrakulchote N, Chen MY, Moehl T, Tsai HH, Zakeeruddin SM, Wu CG, Grätzel M. A new heteroleptic ruthenium sensitizer for transparent dye-sensitized solar cells. *Adv Energy Mater* 2012; 2: 1503-9.
- [22] Definition of stability: the lifetime of cation radical in air.



Scheme 1. Synthetic route of the dyes.

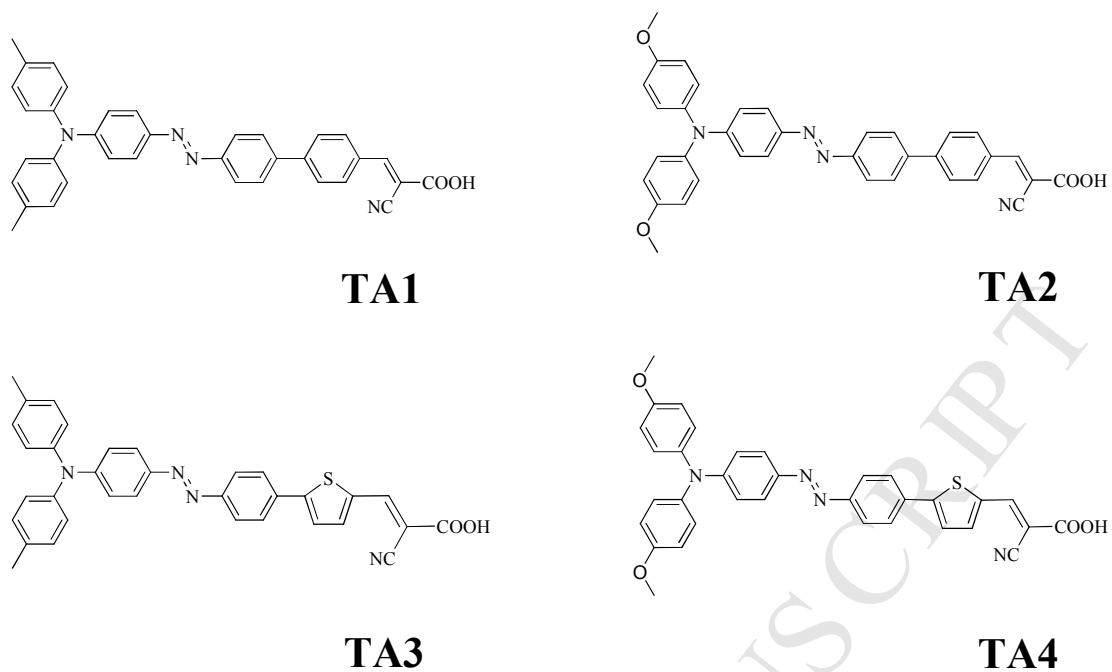


Figure 1. Chemical structures of the azobenzene-bridged materials used in this study.

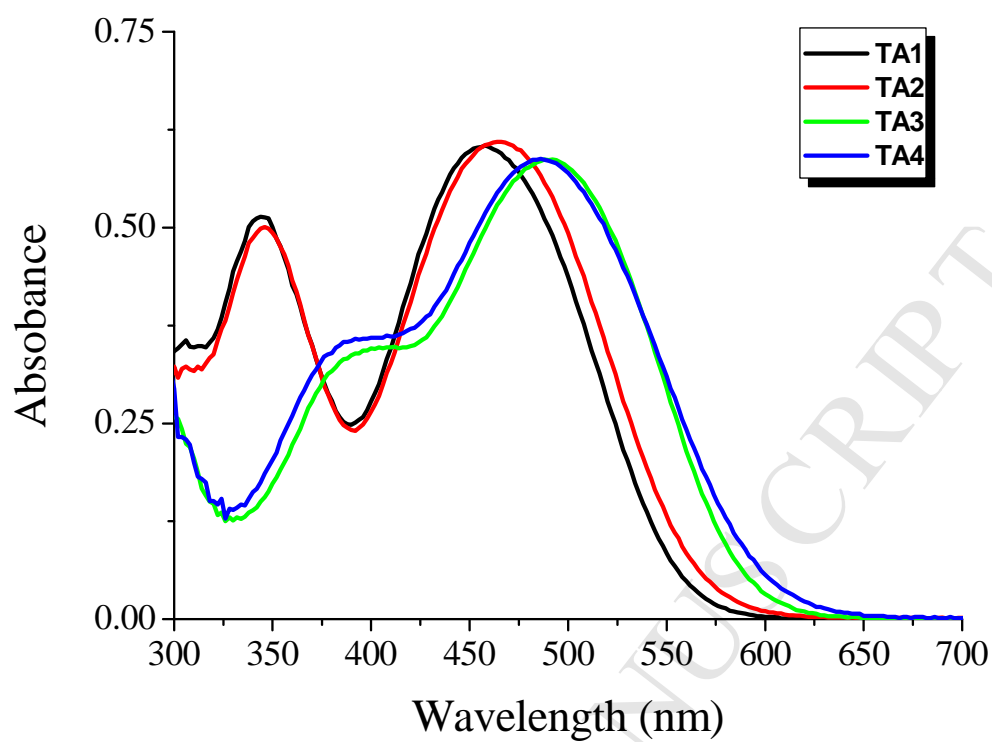


Figure 2. Absorption spectra of the dyes (TA1-TA4) in CH₃CN.

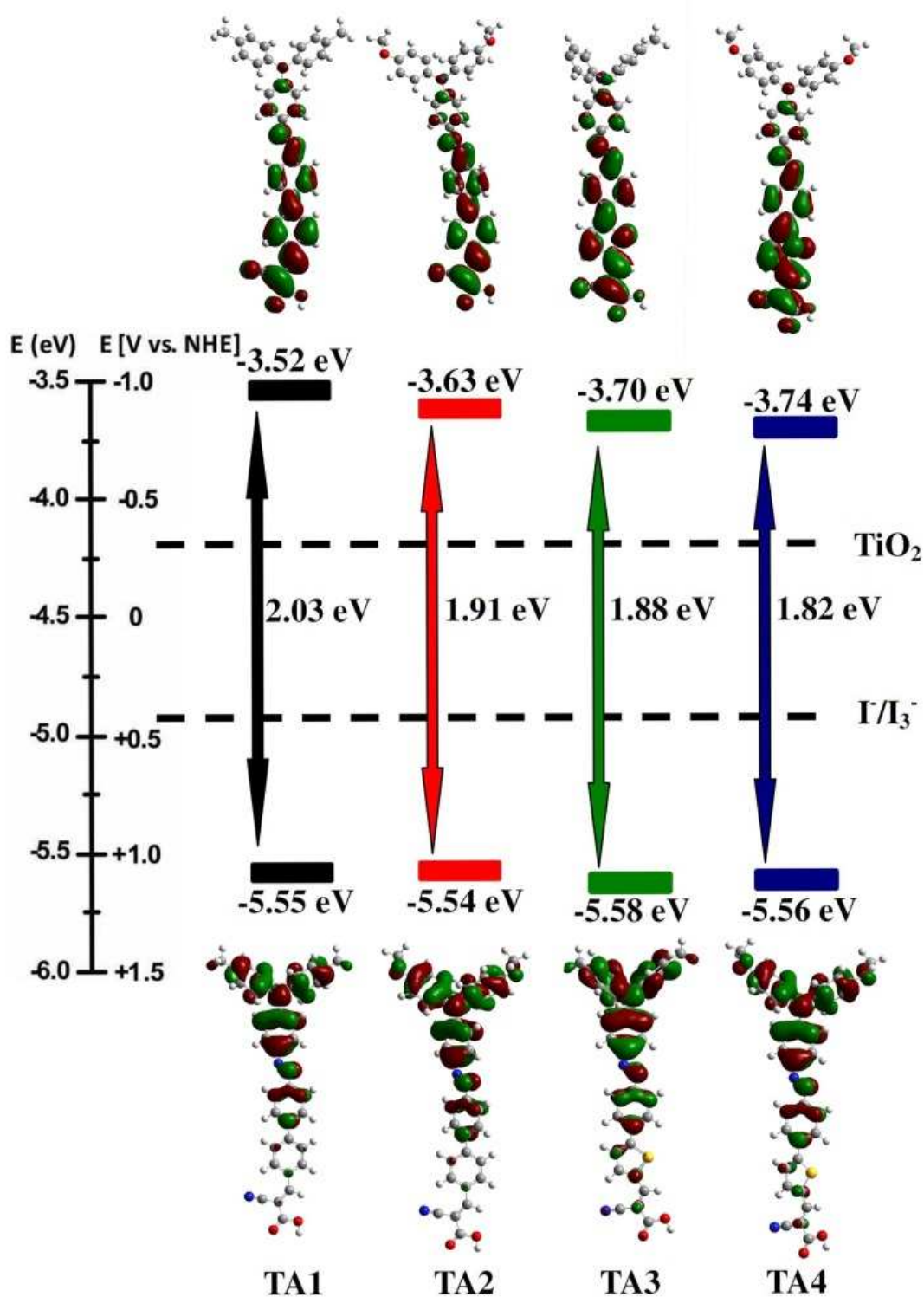


Figure 3. Calculated frontier molecular orbitals and experimental energy level diagram of TA1-TA4 measured in CH₃CN as well as the conduction band of TiO₂ and the redox potential of I/I₃⁻.

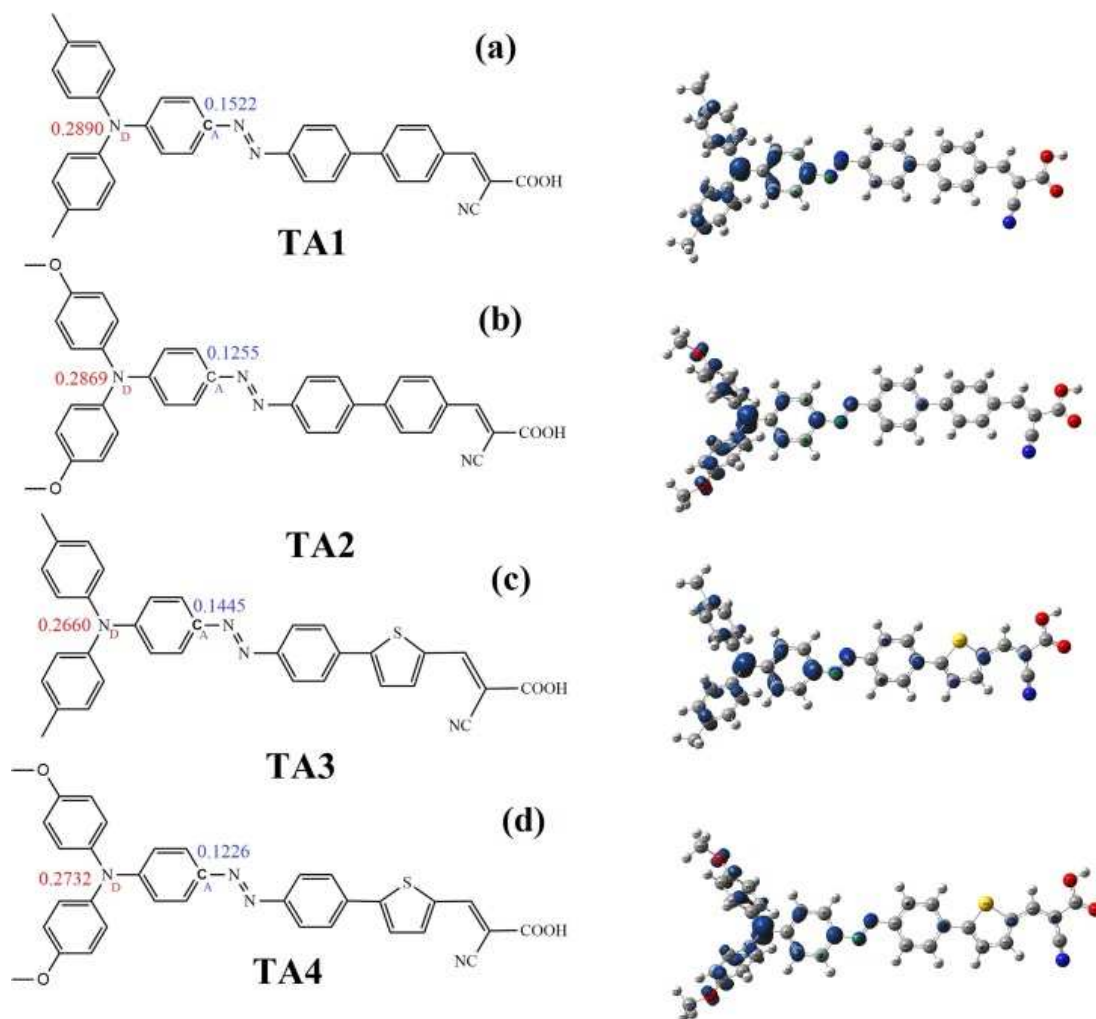


Figure 4. DFT-calculated spin density distribution of (a) **TA1**⁺, (b) **TA2**⁺, (c) **TA3**⁺, and (d) **TA4**⁺. Isovalue: 0.004

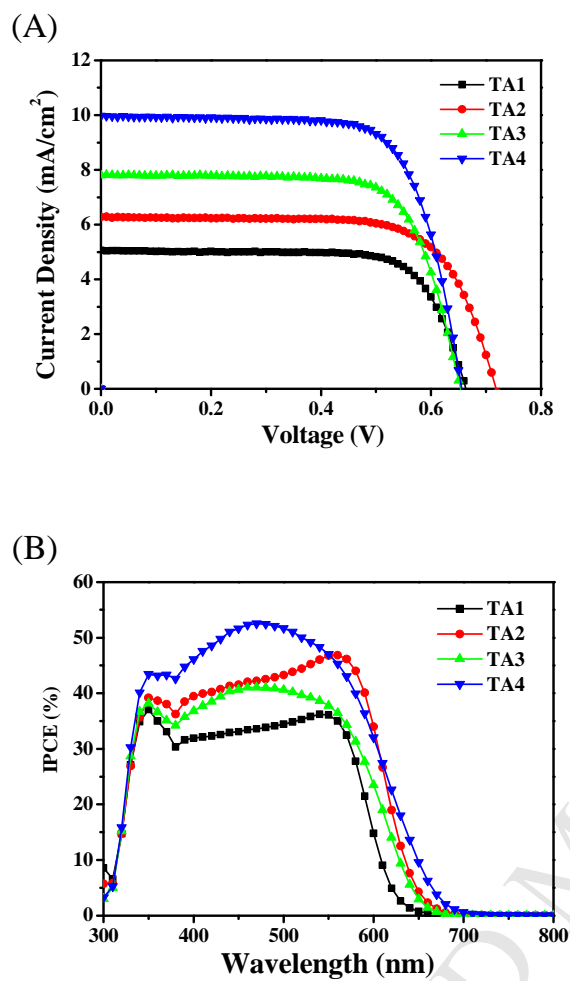


Figure 5. (A) *J-V* curves and (B) IPCE spectra of DSCs sensitized by the dyes TA1-TA4 with electrolytes containing 0.6M BMII, 0.1M LiI, 0.05 M I₂, 0.1 M GuNCS, 0.5 M TBP in dried THF.

Table 1. Peak potentials (V vs. Ag/AgCl) of **TA1-TA4** (determined by square wave voltammetry) in CH₂Cl₂/TBAPF₆.

	Oxidation		Reduction
	2nd	1st	1st
TA1	+1.02	+0.85	-1.66
TA2	+1.40	+0.84	-1.28
TA3	+1.04	+0.88	-1.14
TA4	+1.09	+0.86	could not observed

Table 2. Optical and electrochemical properties of the dyes

Dye	1st $E_{1/2}$ (V vs. Ag/AgCl)	1st $E_{1/2}$ (V vs. NHE)	HOMO (eV) ^b	λ_{onset} (nm)	E_{0-0} (eV) ^c	LUMO (eV) ^d
TA1	+0.85	+1.05	-5.55	610	2.03	-3.52
TA2	+0.84	+1.04	-5.54	650	1.91	-3.63
TA3	+0.88	+1.08	-5.58	660	1.88	-3.70
TA4	+0.86	+1.06	-5.56	680	1.82	-3.74

a. $\text{FeCp}_2^{+/0} = +0.49$ V in $\text{CH}_2\text{Cl}_2/\text{TBAPF}_6$.

b. The HOMO energy level was calculated from the half-wave potential during oxidation according to the empirical formula: $E_{\text{HOMO}} = -(E + 4.5)$ V by assuming the energy level of ferrocene to be - 4.5 eV below vacuum level. (E (V) vs. NHE)

c. The gap energy level was calculated from the onset wavelength of the UV-Vis spectrum according to the empirical formula: $E_{\text{gap}} = 1240/\lambda_{\text{onset}}$

d. $\text{LUMO} = \text{HOMO} + \text{gap}$

Table 3. Calculated ionization potentials (IP, eV) and HOMO-LUMO gaps (eV).

Index	IP (eV)	HOM O (eV)	LUMO (eV)	HOMO-LUMO gap (eV)
TA1	6.13	-5.09	-2.68	2.41
TA2	5.93	-4.94	-2.63	2.32
TA3	6.13	-5.15	-2.83	2.32
TA4	5.95	-5.00	-2.77	2.23

Calculated in the gas phase. B3LYP/6-31G(d,p)

Table 4. Photovoltaic Performance Data of **TA** Dyes.

Dye	Jsc (mA/cm ²)	Voc (V)	FF	PCE (%)
TA1	5.40	0.662	0.715	2.56
TA2	6.83	0.704	0.718	3.45
TA3	7.81	0.654	0.723	3.69
TA4	9.92	0.662	0.728	4.78

Highlights

- A series of novel azobenzene-based dyes were synthesized.
- The stability order of these four dyes cation radicals was found to be **TA4 > TA3 > TA2 > TA1** in air.
- The new record on PCE with using azobenzene as the π -spacer unit was achieved.